Scientific Research Publishing

Open Journal of Geology, 2026, 16(4), 197-213
https://www.scirp.org/journal/ojg
ISSN Online: 2161-7589
ISSN Print: 2161-7570

Petrographic and Geochemical Characters of the Metasediments and Granitoids in the Dimbokro Region (Centre-East Côte d'Ivoire)

Diakite Sekou[1*], Pria Koffi Kossonou Jean-Marie[2], Adingra Martial Pohn Koffi[3], Gballou Clovis Blanchard[3], Allialy Marc Ephrem[3]

[1]Laboratoire des Sciences, Ressources Minérales et Energétiques (LSRME), Ecole Doctorale Sciences, Technologie et Agriculture Durable (ED-STAD), Université Félix Houphouët-Boigny Abidjan-Cocody, Abidjan, Côte d'Ivoire
[2]Jean Lorougnon Guédé University (University of Daloa), Daloa, Côte d'Ivoire
[3]Laboratory of Geology, Mineral and Energy Resources (LGRME), Faculty of Earth Science and Mineral Resources, Félix Houphouët Boigny University, Abidjan, Côte d'Ivoire
Email: *diakitesekou07@gmail.com

How to cite this paper: Sekou, D., Jean-Marie, P.K.K., Koffi, A.M.P., Blanchard, G.C. and Ephrem, A.M. (2026) Petrographic and Geochemical Characters of the Metasediments and Granitoids in the Dimbokro Region (Centre-East Côte d'Ivoire). *Open Journal of Geology*, **16**, 197-213.
https://doi.org/10.4236/ojg.2026.164011

Received: March 10, 2026
Accepted: April 20, 2026
Published: April 23, 2026

Abstract

This study examines the petrographic and geochemical characteristics of the metasediments and granitoids in the Dimbokro region. Petrographic characterisation reveals that the study area is dominated by two major lithological units: metasedimentary rocks (mica schists, metagrauwackes and quartzites) and a suite of intrusive granitoids (biotite granites, granodiorites and tonalites). Chemical analysis indicates that these granitoids are of type I, and the chemical weathering index (CWI) values for the metasediments range from 54.3 to 79.1, indicating moderate weathering of the parent rocks, suggesting protoliths of intermediate to felsic igneous composition. Rare earth element patterns show marked LREE enrichment over HREE, with (La/Yb) N ratios ranging from 7.2 to 18.6 in the metasediments and from approximately 15 to 110 in the granitoids, reflecting varying degrees of crustal fractionation. Negative Nb-Ta anomalies in multi-element spectra indicate that both lithological units were formed in a subduction-related tectonic setting. These two lithological units form part of the Palaeoproterozoic Birimian evolution of the West African Craton.

Keywords

Dimbokro, Bassin of Comoe, Metasediments, Granitoids, Petrography, Geochemistry

1. Introduction

The West African Craton (WAC) is one of the major cratonic domains of the Afri-

can continent, whose lithological units can be grouped into four major groups: formations involved in Pan-African orogenesis, Birimian and Tarkwian formations, Liberian or Archaean formations, and Leonian formations. Seventeen (17) Birimian furrows run through the Comoé Basin in Côte d'Ivoire. They consist of greenstone belts, granitoids, volcano-sedimentary belts and sediments deposited during the Eburnean orogeny [1] [2]. The study area is located in the south-eastern part of the Comoé basin, which is heavily involved in the study and evolution of the basin's metasedimentary rocks. Several petrographic and geochemical studies have proved particularly effective in obtaining information on the depositional setting and provenance of Archaean and Proterozoic sediments [3]-[11] among many others. Following in the footsteps of these authors, this study presents a petrographic and geochemical characterisation of the metasediments and granitoids from the Dimbokro region, which remain poorly documented in the literature. The specific objectives are as follows: 1) to determine the petrography of these rocks; 2) to classify the metasediments and identify their provenance; 3) to identify the geodynamic environment of these rocks.

2. Geological Context

The Ivory Coast belongs to the southern part of the West African craton, known as the Leo-Man ridge. It is composed of an Archaean core (3600 - 2500 Ma) located to the west, in contact with a Paleoproterozoic domain located to the east. These two domains are separated by the Sassandra fault [12]. The Birmi domain comprises three lithological groups: volcanic belts, sedimentary basins and granito-gneiss massifs.

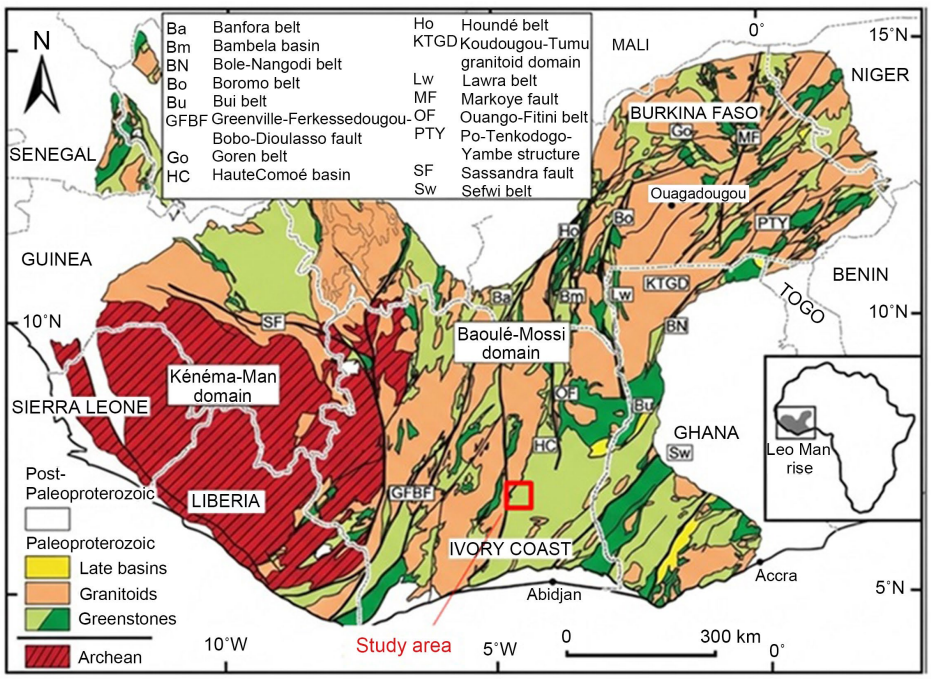

Figure 1. Simplified geological map of the Man-leo Ridge in Man [13], showing the study area.

The study area is located in the central-eastern part of the Comoé Basin (**Figure 1**), one of the largest Birmiens sedimentary basins in the region. This basin is mainly siliciclastic, composed of grauwackes and mudstones deposited in deep water under a turbiditic regime [13] [14]. Episodes of submarine volcanism are also documented locally, as well as occasional carbonate levels. The lithostratigraphy of the Comoé unit is mainly composed of quartzites, basic to acidic volcanic rocks, schists and sandstones [15] resting unconformably on an antebirimian granito-migmatitic basement. According to [16] (**Figure 2**), the geology of the study area consists of biotite and/or muscovite granite, biotite metagranite, granodiorite, and metarenites dominating over metasiltites. These geological units have been affected by marked polyphase deformation.

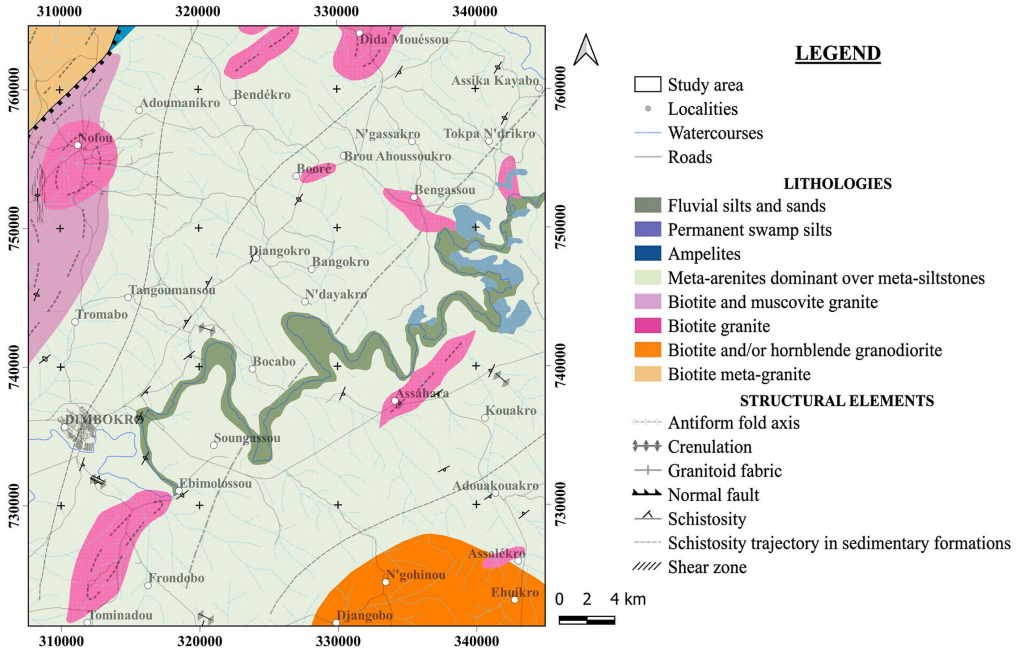

Figure 2. Geological map of the study area and location of the metasediments and granitoids studied (Excerpt from [16]).

3. Analytical Method

Fourteen (14) rock samples were selected during various field missions. Thin sections of these metasediments were prepared and studied at the Bedrock Geology and Metallogeny Laboratory at Félix Houphouët-Boigny University in Abidjan. Some of these samples were sent to the Bureau Veritas Côte d'Ivoire mineral analysis laboratory to determine their major and trace element composition by atomic emission spectrometry (ICP-AES) and mass spectrometry (ICP-MS) (**Table 1**). They were successively crushed by jaw crushers and then roller crushers. The powders were divided by quartering using an equiproportional separator. Their particle size was reduced to 70 - 80 µm. Chemical analyses were performed on 10 grams of rock powder and fifty-six chemical elements were measured. These were the following elements: - Major elements (12): SiO_2, Al_2O_3, Fe_2O_3, CaO, MgO,

Na_2O, K_2O, TiO_2, MnO, P_2O_5, Cr_2O_3, and loss on ignition (LOI). Eleven elements were analyzed by atomic emission spectrometry (ICP AES), while Cr_2O_3 was quantified by mass spectrometry (ICP MS); Base metals (8): Ag, Co, Cu, Mo, Ni, Pb, Zn, and Cd obtained by a (AQ 200). This procedure is followed by atomic emission spectrometry (ICP AES) to determine the content; Volatile elements (6): As, Bi, Hg, Sb, Se, and Be were first digested using Aqua Regia (AQ 200), then quantified using inductively coupled plasma mass spectrometry (ICP-MS); Trace elements and rare earth elements (REE) (30 elements): Ba, Ce, Cs, Dy, Er, Eu, Ga, Gd, Hf, Ho, La, Lu, Nb, Nd, Pr, Rb, Sm, Sn, Sr, Ta, Tb, Th, Tl, Tm, U, V, W, Y, Yb, and Zr are first subjected to lithium-boron fusion before being dissolved. Finally, inductively coupled plasma mass spectrometry (ICP MS) was used to quantify them.

Table 1. Chemical composition of metasediments and granitoids.

	Metasedimentary rock							Granitoid rock						
Sample	**DIM2**	**DIM2-1**	**DIM 3**	**DIM7-3**	**DIM4**	**DIM5**	**DIM5-1**	**DIM2-2**	**DIM2-3**	**DIM2-4**	**DIM7**	**DIM7-1**	**DIM7-2**	**DIM7-4**
SiO_2	73.96	87.56	63.08	71.98	68.4	62.8	63.4	73	73.2	72.9	66.1	68.4	61.51	62.08
Al_2O_3	12.1	6.32	14.98	14.21	14.7	17.09	17.5	14.7	14.7	14.4	16.1	15.5	14.8	14.21
Fe_2O_3	5.63	2.88	6.14	5.12	5.25	7.01	7.04	1.47	1.19	1.66	4.05	3.71	5.03	4.45
CaO	0.28	0.08	3.21	0.21	1.38	2.08	1.31	1.24	0.69	1.03	3.4	3.05	3.51	3.78
MgO	1.12	0.4	3.4	1.07	2.01	6.309	2.69	0.32	0.23	0.38	1.75	1.17	2.34	2.38
Na_2O	2.72	0.29	3.65	3.9	3.35	2.37	2.3	4.13	3.79	4.07	4.35	4.45	3.57	4.01
K_2O	1.45	1.51	3.05	1.5	1.83	3.41	2.9	4.58	5.08	4.97	2.68	2.85	2.9	2.8
MnO	0.09	0.02	0.08	0.02	0.07	0.68	0.08	0.03	0.04	0.03	0.06	0.06	0.08	0.07
TiO_2	0.55	0.2	0.62	0.53	0.56	2.67	0.7	0.18	0.11	0.27	0.49	0.45	0.55	0.49
P_2O_5	0.05	0.02	0.31	0.12	0.12	0.08	0.22	0.07	0.14	0.08	0.21	0.16	0.22	0.22
Cr_2O_3	0.02	<0.01	0.02	0.02	0.02	0.14	0.02	0.01	0.02	0.01	0.01	0.01	0.01	0.01
LOI	2.37	1.23	1.71	1.85	2.64	0.02	2.23	0.32	0.64	0.36	0.65	0.13	5.73	6.09
TOTAL	100.34	100.51	100.25	100.53	100.33	105.66	100.39	100.05	99.83	100.16	99.85	99.94	100.25	100.59
Ba	646	448	1176	332	474	547	726	1113	387	869	1276	1013	1185	1097
Be	5	<1	2	4	4	2	3	4	2	1	5	2	<1	4
Co	39.5	8.5	20	6.1	17	20.5	22.3	2.3	1.4	3.7	11.2	9.3	14	12.5
Cs	3	3.3	1.7	2	3.3	53.7	3.5	8.6	22.7	7.3	38.5	2.8	2.7	2.9
Ga	11.6	5.4	15.2	13.7	16.4	19.9	20.6	19.9	25.5	23.2	19.8	19.9	16.2	15.8
Hf	4.3	2	3.6	4	4.1	4.5	3.5	3.6	2.5	4.8	3.9	4	3.8	3.4
Nb	4.9	2.3	5.5	5.7	5.4	8.7	6.8	4.9	10.9	6.6	4.7	5.4	5.4	4.6
Rb	54.4	53.9	74.1	61.4	76.4	190.1	93.4	213.3	417	252.9	125.9	85.7	87.8	92.6
Sn	<1	<1	<1	1	<1	1	<LD	<1	3	<1	<1	<1	<1	<1
Sr	128	56.6	878.4	275	353.8	352.7	241.6	497.1	88	323.6	858.1	659.4	823.9	479.3
Ta	0.4	0.2	0.5	0.5	0.5	1	0.4	0.9	1.6	0.7	0.4	0.6	0.4	0.4
Th	5.1	2.1	5.2	4.8	5.2	5.6	4.3	13.9	10.6	10.3	5	6.7	5.2	4

Continued

U	1.2	0.5	1.2	1.2	1.2	1.6	1.3	5.7	6.9	1.9	3.1	1.3	2.3	1.5
V	104	42	108	84	85	126	111	10	19	18	88	58	82	72
W	3.5	0.8	<0.5	1	1.6	<0.5	0.6	<1	0.6	<1	3.1	<0.5	10.2	2.4
Zr	178.2	73.6	136.4	145.7	156.6	160.6	145	130.3	73.1	186	135.7	148.8	144.4	126
Y	27.5	7.7	13.8	18.4	11.1	18.2	15.6	68.2	7.8	4.3	9.1	8.1	13	10.7
La	34.5	21.3	31.4	27	25.1	28.9	24.6	155.3	15.3	35.8	28.1	30.4	34.8	28.2
Ce	51.6	32.9	65.6	54.7	46.8	58.2	52.6	203.5	27.6	65.8	65	58.3	68.4	55
Pr	6.37	4.41	7.59	6.35	5.3	7.02	5.75	23.97	3.01	7.05	7.15	5.99	8.13	6.58
Nd	24.3	15.8	30.8	25	19.7	26.3	22.4	92.8	11.3	22.7	29.2	21.7	31.9	25.4
Sm	4.38	2.65	5.31	4.5	3.51	4.97	3.92	14.16	2.21	3.16	4.99	3.51	5.09	4.1
Eu	1.2	0.69	1.5	1.1	0.95	1.34	1.1	3.44	0.28	0.71	1.3	1.01	1.31	1.13
Gd	4.75	2.42	4.02	3.98	2.88	4.29	3.42	15.13	1.81	1.79	3.33	2.64	4.03	3.03
Tb	0.66	0.33	0.5	0.54	0.42	0.61	0.52	1.84	0.28	0.2	0.39	0.31	0.47	0.4
Dy	3.87	1.78	2.68	3.18	2.3	3.45	2.75	9.55	1.47	0.85	1.7	1.45	2.55	2.11
Ho	0.8	0.34	0.5	0.6	0.46	0.68	0.64	1.84	0.28	0.14	0.29	0.25	0.47	0.39
Er	2.36	0.82	1.34	1.69	1.26	1.96	1.78	4.77	0.8	0.32	0.85	0.76	1.44	1.06
Tm	0.3	0.13	0.21	0.24	0.19	0.3	0.26	0.57	0.12	0.04	0.12	0.1	0.18	0.12
Yb	1.8	0.79	1.23	1.68	1.37	2.13	1.8	0.44	0.87	0.32	0.71	0.65	1.34	0.89
Lu	0.3	0.11	0.19	0.25	0.21	0.32	0.27	0.49	0.13	0.04	0.11	0.11	0.18	0.13
Mo	<0.1	0.4	<0.1	0.2	0.3	0.2	0.3	0.4	0.8	0.5	1.1	0.6	0.1	3.2
Cu	25.1	16	24	16.1	23.6	10.4	30.7	5.3	10.8	5.6	19.4	14.6	23.1	13.7
Pb	1.8	4.4	4.9	3.2	5.2	3	2.1	5.6	9.3	9.1	4.1	2.4	7.3	7.6
Zn	48	18	48	57	57	57	84	33	20	32	65	52	50	29
Ni	73.1	21.7	37.9	50.4	38.7	48.7	53.5	2.7	1.7	3.8	19.2	7.4	23	18.1
As	1.2	1.6	0.8	5.1	0.7	0.7	<1	<1	<1	<1	<1	<1	4.8	0.9
Cd	<0.1	<0.1	<0.1	<0.1	<1	<0.1	<1	<1	<1	<1	<1	<1	<0.1	<0.1
Sb	0.2	0.2	0.3	0.1	<1	<0.1	<1	<1	<1	<1	<1	<1	0.3	0.1
Bi	<0.1	0.1	<0.1	0.1	<1	0.3	0.2	<1	1	0.1	0.8	<1	<0.1	0.1
Ag	<0.1	<0.1	<0.1	<0.1	<1	<0.1	<1	<1	<1	<1	<0.1	<1	<0.1	<0.1
Au	1.9	2.4	1.4	4.9	<1	0.3	<1	<1	<1	<1	<0.5	<1	30.2	0.7
Hg	<0.01	<0.01	<0.01	<0.01	<1	<0.01	<1	<1	<1	<1	<1	<1	<0.01	<0.01
Tl	<0.1	<0.1	<0.1	<0.1	<1	0.9	0.2	0.4	0.2	0.1	0.5	0.4	<0.1	<0.1
Se	<0.5	<0.5	<0.5	<0.5	<1	<0.5	<1	<1	<1	<1	<1	<1	<0.5	<0.5

4. Results

4.1. Petrographic Descriptions

4.1.1. Metasediments

1) Mica schist

The widely distributed schists (32% of the total) are always in an advanced state

of weathering and mainly contain sericite and pyrite, sometimes in significant quantities. These schists may be enriched with sandy elements (mainly quartz). They are traversed by large quartz veins, which are often gold-bearing. Originally grayish to greenish-gray, they give rise to outcrops of laterites that have retained their original schistosity, or yellow and brown clays with whitish, reddish, and purplish streaks. Rare outcrops of fresh mica schist have nevertheless been observed near the towns of Dimbokro and Ahua (**Figure 3(a)**). The schistosity affecting the rock is oriented NE-SW and dips to the northwest. In thin sections, the rock has a grano-lepidoblastic texture highlighted by mineral foliation with alternating surmicacous beds and quartz-feldspar beds. The surmicacous beds consist of brown biotite, sometimes chloritized (green biotite), and muscovite, accompanied by interstitial crystals of xenomorphic quartz (**Figure 3(b)**).

2) Metagraywacke

Metagraywackes are observed in the bed of the N'Zi River in the village of Broukro, where they form alignments of sometimes thin bands (**Figure 3(c)**). To the naked eye, the rock is dense, very coherent, dark in color, schistose in appearance, and generally derived from sandstones with relatively abundant cement (20%). Under the microscope, samples taken from the matrix, which have a granolepidoblastic texture dominated by the orientation and interlocking of phyllitic minerals, show the following mineralogical composition (**Figure 3(d)**): Quartz constitutes the bulk of the rock, often with very frequent and intense rolling extinction, indicating strong deformation. Micas (muscovite and biotite) are very abundant, forming elongated aggregates and continuous bands that align clearly to define the foliation. Chlorite is often associated with the alteration of biotite. Plagioclase crystals are less abundant than quartz and are generally unaltered. Opaque minerals are accessory minerals in the slide, appearing as small, scattered opaque black grains, probably iron oxides. The composition of these metagrauwackes, a mixture of quartz, feldspars, and micas in a fine matrix, is consistent with that of Birimian grauwackes described in other basins in the region [13] [11].

3) Quartzite

Macroscopically, this rock appears as a beige-grayish to white block with a massive, granular appearance (**Figure 3(e)**). The texture is clearly granular, with grains visible to the naked eye, suggesting recrystallization. Under the microscope, the rock has a granoblastic texture, characterized by an overwhelming dominance of quartz (**Figure 3(f)**). The quartz grains are medium to coarse in size, generally xenomorphic to subautomorphic in shape, and show rolling extinctions and mechanical twins, evidence of the deformation undergone during metamorphism. The grain joints are sutured and interlocked, indicating complete recrystallization of the original sediment. Accessory minerals are present in very small quantities, appearing as fine colored (yellow, orange, brown) or opaque patches scattered between the quartz grains. These traces of oxides may correspond to minute amounts of clays or iron oxides present in the sedimentary protolith (pure quartz sandstone) prior to metamorphism.

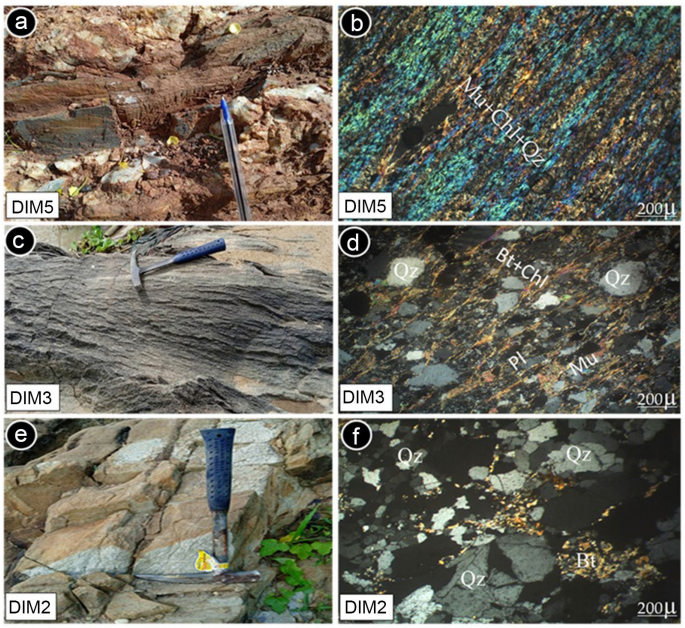

Figure 3. Macroscopic and microscopic aspects: Mica schist. (a) and (b); Metagraywacke (c) and (d); Quartzite (e) and (f). Qz: quartz. Pl: plagioclase. Bt: biotite. Mu: muscovite. Chl: chlorite. Op: opaque.

4.1.2. Nature and Origin of Metasediments

The chemical compositions of the seven samples analyzed are presented in (**Table 1**). SiO_2 contents vary between 62.8% and 87.6%, with the highest values in quartzites (DIM2-1: 87.6%) and the lowest in mica schists and metagrauwackes. Al_2O_3 contents ranged from 6.3% to 17.5%, with the highest values found in the mica-rich mica schists (DIM5 and DIM6). Fe_2O_3 concentrations ranged from 2.88% to 7.04%. CaO contents are generally low (0.08% to 3.21%), with the exception of sample DIM3 (3.21%), which also has a high MgO content (3.40%). This last sample could reflect a higher proportion of ferromagnesian minerals or carbonates in the protolith. Alkalies ($Na_2O + K_2O$) vary between 1.74% and 6.70%, with a K_2O/Na_2O ratio between 0.41 and 5.21. Loss on ignition (LOI) is moderate (1.2 to 2.6% for most samples), with the exception of DIM6 (LOI ≈ 0.02%), which reflects hydration linked to the presence of phyllitic minerals.

The [17] diagram (**Figure 4(a)**) indicates that all samples fall within the range of sedimentary rocks with a meta-aluminous to peraluminous character, consistent with protoliths of pelitic to greywackeous composition. According to [18] classification diagram: Log (Fe_2O_3/K_2O) as a function of Log (SiO_2/Al_2O_3) (**Figure 4(b)**), the samples are mainly distributed in the shale and wacke fields. Only one sample (DIM2-1) is positioned in the quartzarenite field, consistent with its dominant quartz content (SiO_2 = 87.6%). This distribution is characteristic of sediments in Birimian basins, where shales and grauwackes coexist with subordinate sandstone levels [9] [11].

The chemical weathering index (CWI = $[Al_2O_3/(Al_2O_3 + CaO^* + Na_2O + K_2O)] \times 100$; [19] was calculated for each sample. The values obtained range from 54.3

to 79.1, indicating low to moderate alteration of the source rocks. The highest values (DIM2-1: 79.1; DIM2: 66.4; DIM5: 66.8) correspond to samples richer in Al and poorer in CaO + Na_2O, indicating more advanced hydrolysis of feldspars in the source rock or longer transport of detrital material. The lower values (DIM3: 54.3; DIM6: 57.6) suggest a less altered source, probably slightly to moderately transformed igneous rocks.

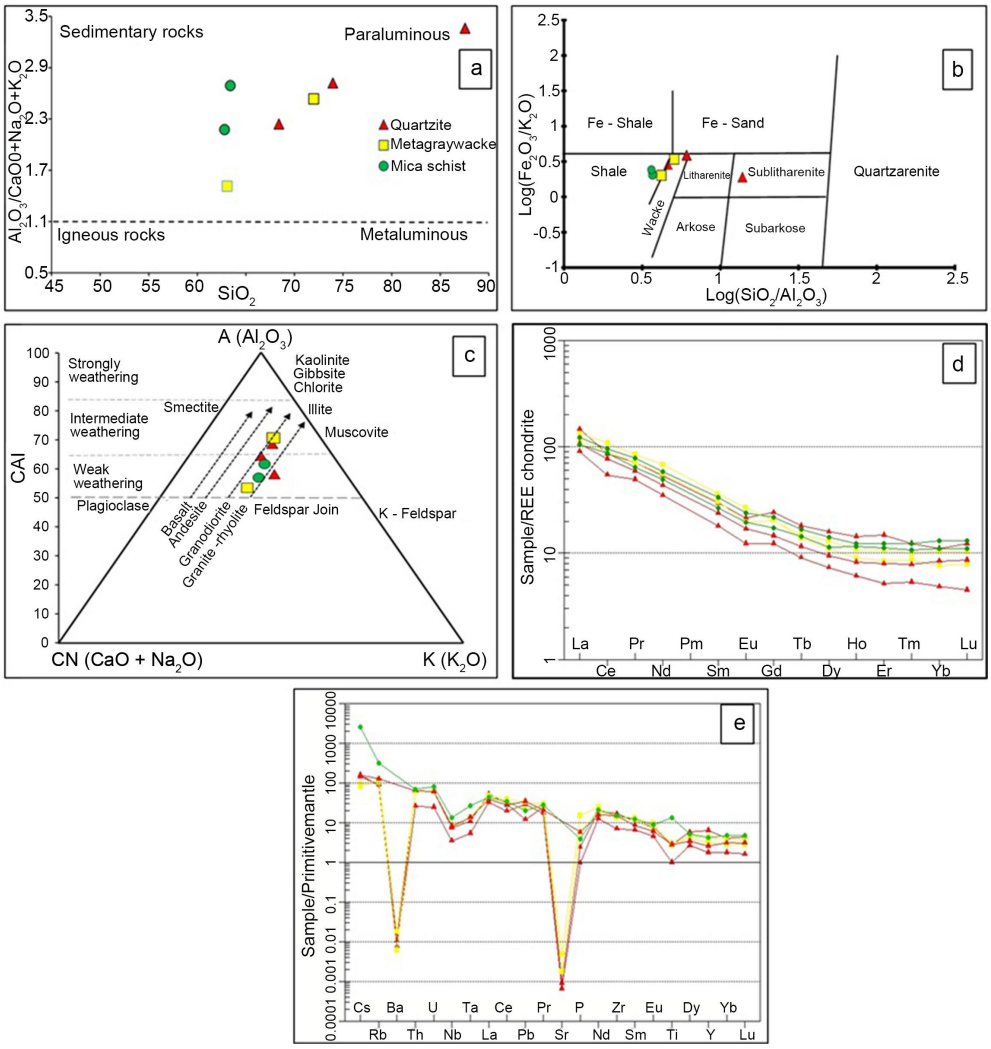

Figure 4. (a) [17] discrimination diagram; (b) Log (Fe_2O_3/K_2O) versus log (SiO_2/Al_2O_3) diagram [18]; (c) A-CN-K diagram; (d) Chondrite normalized rare earth spectra and (e) Multi-element diagrams of metasedimentary rocks normalised to the primitive mantle [21] applied to metasediments from the Dimbokro region.

The A-CN-K ternary diagram (A = Al_2O_3, CN = CaO + Na_2O, K = K_2O, in molar proportions) by [20] (**Figure 4(c)**) indicates that the protoliths of the studied metasediments range from granodiorites and granites. The alteration trajectory of the samples is consistent with an evolution from source rocks of intermediate to felsic composition, slightly to moderately altered.

The rare-earth spectra [21] (**Figure 4(d)**) of the Dimbokro metasediments show

a marked enrichment in light rare earth elements (LREE) relative to heavy rare earth elements (HREE), with (La/Yb) N ratios ranging from 7.2 to 18.6. The mica schists exhibit the most pronounced fractionation, indicating a source dominated by felsic crustal materials, whilst the metagrauwacks, with more moderate values, reveal a more significant contribution from a mafic volcanic source. The europium anomaly is slightly negative for the majority of samples (Eu/Eu*: 0.67 - 0.95), indicating a source that has undergone plagioclase differentiation, typical of Eburonian granitoids and TTGs. Only sample DIM6, with a positive anomaly (Eu/Eu* ≈ 1.12) and high MgO and TiO_2 contents, stands out due to a greater contribution from a mafic source to the cumulate. Overall, these spectra confirm a mixed sedimentary supply from intermediate to felsic crustal sources of arc affinity, within the context of the Eburnean orogeny.

The multi-element spectra normalized to the primitive mantle of [21] (**Figure 4(e)**) show profiles that are generally consistent with each other. There is a relative enrichment in elements with large ionic radii (LILE: Rb, Ba, K) and a marked depletion in elements with high ionic charges (HFSE: Nb, Ta, Ti). This depletion in Nb-Ta relative to La, Th, and Ce is characteristic of magmas and sediments derived from sources linked to a subduction zone [3] [22]. The positive Ba anomaly (particularly in DIM3: 1176 ppm) may be linked to a high detrital component of potassium feldspars, or to diagenetic processes. The rare earth elements show little differentiation between LREE and HREE, with La/Yb (N) values ranging from approximately 10 to 25, suggesting a continental crustal source.

4.1.3. Geotectonic Environment of Metasediments

The K_2O/Na_2O diagram as a function of SiO_2 by [23] (**Figure 5**) is used to discriminate the geotectonic environment of detrital sediment deposition. In this diagram, the Dimbokro samples are distributed between the fields of the oceanic island arc margin and the active continental margin. This bipartition is consistent with the results obtained in other areas of the Comoé Basin [24] and in comparable Birimian basins in Ghana [11] [25].

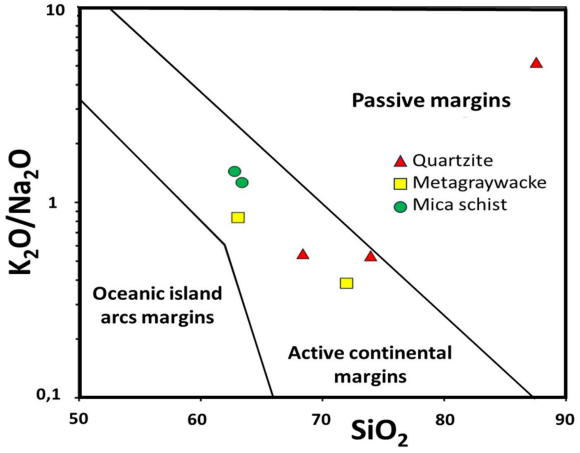

Figure 5. K_2O/Na_2O discrimination diagram based on SiO_2 in the geotectonic context of metasediments, according to [23].

The negative Nb-Ta anomaly observed in the multi-element spectra reinforces this interpretation. It indicates that the sediments were supplied, at least in part, by igneous rocks associated with an arc or active margin context, rather than an oceanic ridge or hotspot context [26] [27].

4.2. Granitoids

4.2.1. Petrographic Data

1) Biotite granite

These are fairly dark-coloured, medium-grained granites (**Figure 6(a)**). They are much more widespread within the study area and are mostly calcic. They outcrop as small massifs shaped by foliation to the south-west of Ebimlossou and at Dida Mouessou, along the Dimbokro-Bocanda axis, where they form a sacred heritage site. Their textural characteristics and their map boundaries intersecting the overlying strata suggest a syn- to post-S2 emplacement. Microscopic examination reveals plagioclase, sometimes zoned with a more calcic and retromorphosed core, as well as quartz in xenomorphic patches with undulating extinction. Biotite is the main ferromagnesian mineral, forming brown lamellae exhibiting marked pleochroism (brown to brown-green). The alteration phases include chlorite and epidote (pistachite) resulting from the alteration of biotite, sericitisation of the alteration products of the plagioclases, and zircon (pleochroic halo in the biotites) (**Figure 6(b)**).

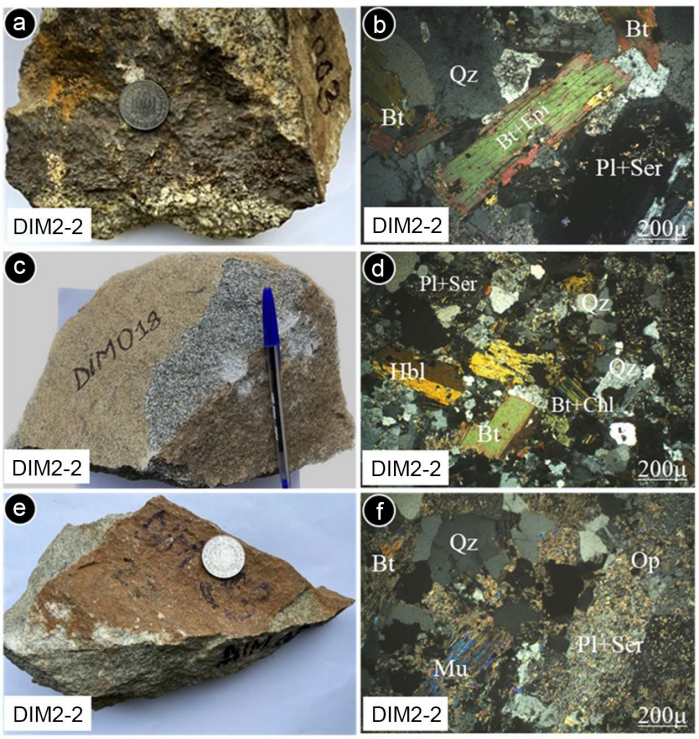

Figure 6. Macroscopic and microscopic aspects: Biotite granite (a) and (b); Granodiorite (c) and (d); Tonalite (e) and (f). Qz: quartz. Pl: plagioclase. Bt: biotite. Mu: muscovite. Hbl: hornblende; Chl: chlorite; Ser: sericite; Op: opaque.

2) Granodiorite

These relatively rare facies consist of medium- to coarse-grained rocks (**Figure 6(c)**). Thin-section analysis reveals a distinct granular texture with a dominant percentage of plagioclase. The plagioclase is more or less retromorphosed (sometimes zoned) and its composition varies from oligoclase to andesine. Microcline occurs either as interstitial material, in small crystals, or as rare phenocrysts. Quartz forms xenomorphic patches with rolling extinction. In natural light, biotite, in large automorphic crystals, is greenish-brown in colour. Rare hornblende crystals have occasionally been observed. Accessory minerals include chlorite, epidote resulting from the destabilisation of biotite, and sericite from the alteration of plagioclases (**Figure 6(d)**).

3) Tonalite

The only tonalite massif has been identified in the central-eastern part of the study area (**Figure 6(e)**). It is dark grey in colour and has a medium to fine grain. At the microscopic level, we observe that microcline is absent or very rare (always less than 3%), compared to the dominant plagioclase (oligoclase). Quartz (over 20%) crystallises in large xenomorphic patches. Green biotite sometimes forms clusters, and there are rare sections of amphibole in the form of elongated greenish prisms. Among the accessory minerals, of note is the local presence of sulphides within the classic suite of accessory minerals (pistachite, chlorite) (**Figure 6(f)**).

4.2.2. Nature and Origin of Granitoids

The major element compositions of the seven samples are shown in **Table 1**. SiO_2 contents range from 61.51% to 73.2%, with higher values for biotite granites (72.9% - 73.2%) and progressively lower values for granodiorites (66.1% - 68.4%) and tonalites (61.51% - 62.08%). The Al_2O_3 contents are relatively stable (14.2% - 16.1%); those of Fe_2O_3 and MgO increase steadily from granites to tonalites, reflecting the overall more mafic composition of the latter. The low TiO_2 values (0.11% - 0.55%) are characteristic of magmatic arc plutonites [28].

In the (Na_2O + K_2O) vs SiO_2 diagram by [29]. (**Figure 7(a)**), the samples are distributed across the fields of granites, granodiorites and tonalites, in perfect agreement with the field petrographic nomenclature. The diagram by [30] indicates that almost all the samples belong to the sub-alkaline series (**Figure 7(b)**). In diagram [31], the rocks are mainly situated in the peraluminous zone (**Figure 7(c)**). The diagram by [17], confirms that these granitoids from the Dimbokro region are of type I, consistent with their petrographic characteristics (presence of amphibole, mafic inclusions, Na_2O/K_2O ratio generally greater than 1 in the tonalites and granodiorites) (**Figure 7(d)**).

The rare-earth spectra, normalised to chondrites according to [27], show a profile with a moderate to steep negative slope, with a marked enrichment in light rare earth elements (LREE) relative to heavy rare earth elements (HREE). The (La/Yb) N ratios vary between approximately 15 and 110 depending on the sample, reflecting varying degrees of fractionation within the suite. The Eu anomaly is generally weak to absent (Eu/Eu* close to 1 for most samples), suggesting that

plagioclase was not a dominant residual phase in the source, or that it did not accumulate significantly during crystallisation. Sample DIM2-2, which is distinguished by particularly high total rare earth element (REE) contents and a strong positive Eu anomaly, may have undergone local enrichment linked to plagioclase accumulation or the introduction of late-stage fluids (Figure 8(a)).

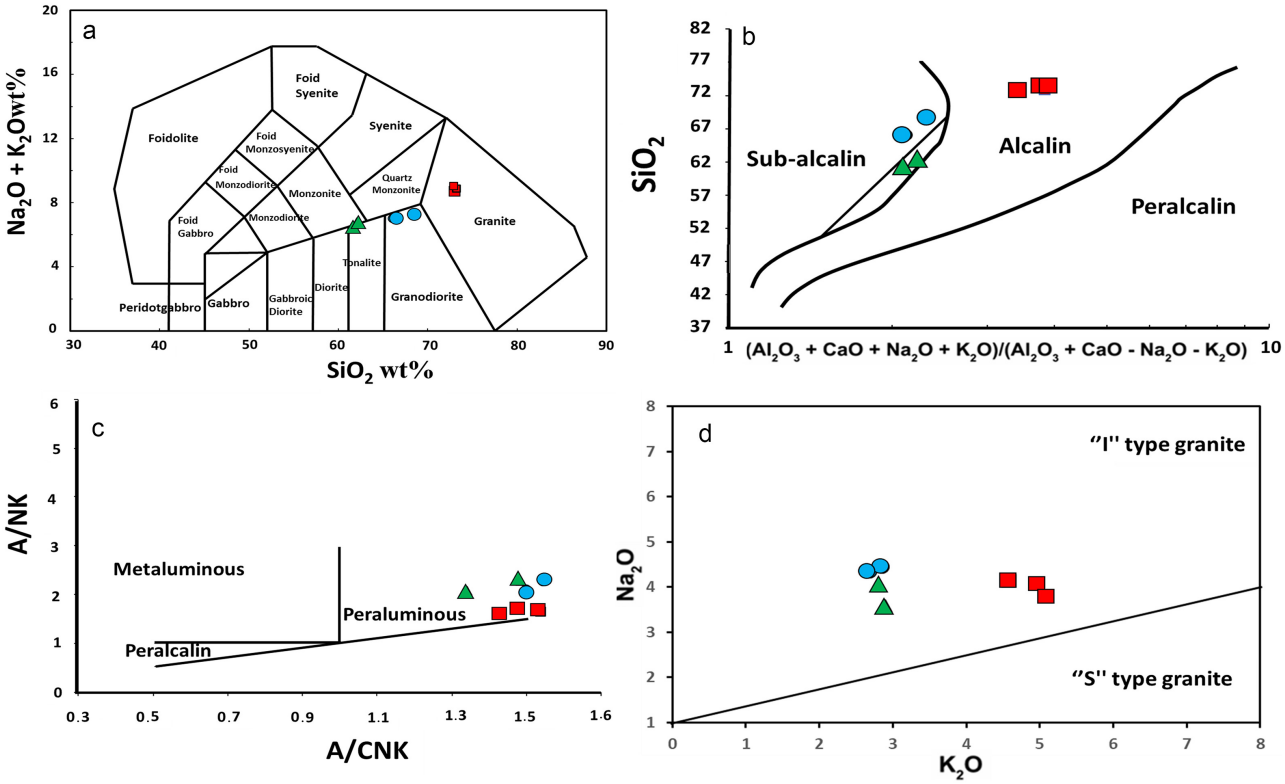

Figure 7. (a) Classification diagram from [29]; (b) Diagram of [30]; (c) Diagram of [31] and (d) Diagram of [17] applied to the granitoids from the Dimbokro region.

Multi-element diagrams normalised to the primitive mantle show, for all samples, a systematic enrichment in large-ion-radius elements (LILE: Cs, Rb, K, Ba) associated with negative anomalies in Nb, Ta, P and Ti. These anomalies in HFSE (high-ion-radius elements) are typical of magmas generated in subduction zones [1] [32]. The negative anomalies in Ti are attributable to the early fractionation of ilmenite and/or sphene in the parent magma (Figure 8(b)).

4.2.3. Geotectonic Environment of Granitoids

In order to understand the geotectonic context of the emplacement of the Dimbokro granitoids, the geochemical data were plotted on the Ta vs Yb discriminant diagram by [33]. All samples fall within the volcanic arc granitoids (VAG) field, with the exception of a few points located on the boundary with the syn-collisional granites (Syn-COLG) field. This distribution is consistent with a subduction setting, likely within an active continental margin or an island arc above a subducted plate (Figure 9).

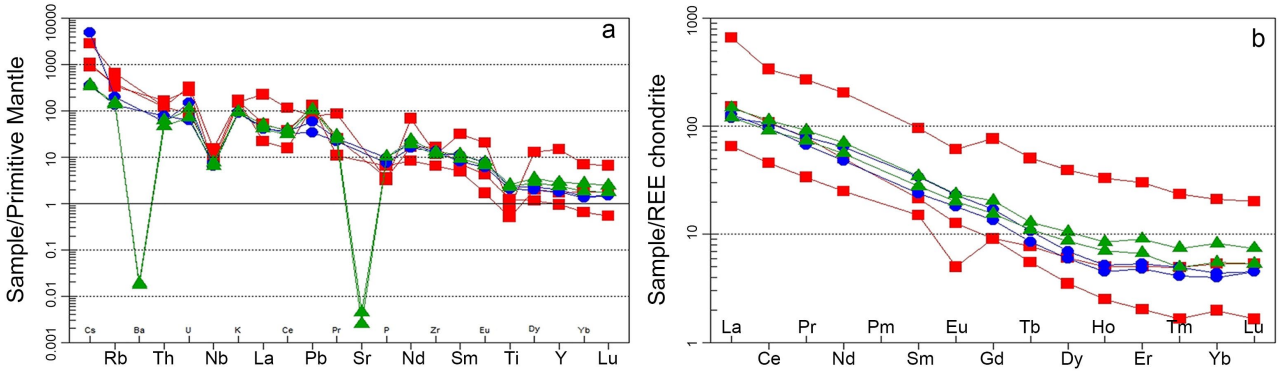

Figure 8. Chondrite normalized rare earth spectra and primitive mantle normalized multi-element spectra applied to plutonites from the Dimbokro region.

5. Discussion

The data obtained from the two lithological units in the Dimbokro region point towards a coherent geodynamic interpretation. On the one hand, the metasediments (mica schists, metagrauwacks and quartzites) represent the older country rock of the study area, constituting a classic siliciclastic turbiditic sequence, analogous to the series described in the major Birimian basins of the region [9] [13]. Their sources are of intermediate to felsic composition. The metasedimentary formations of the Comoé Unit do not originate from the destruction of a volcanic domain, but from the erosion of a granitoid-migmatitic basement, thus generating material composed of quartz and feldspar, with few or no lithic elements [15].

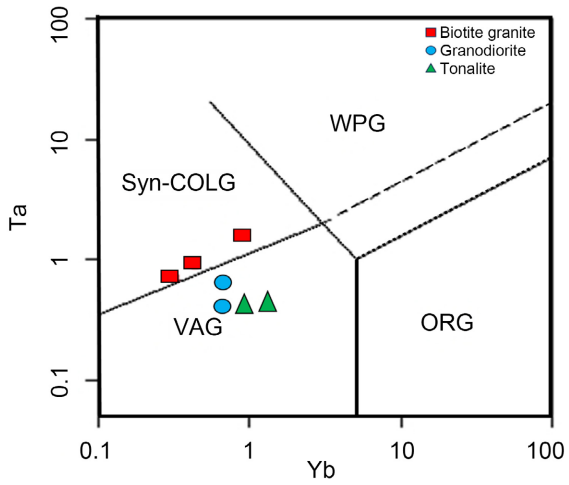

Figure 9. Ta vs Yb diagram from [33] applied to granitoids from the Dimbokro region.

Furthermore, intrusive granitoids (biotite granites, granodiorites and tonalites) exhibit the geochemical characteristics typical of magmas generated in a subduction setting. Compared with the granitoids of the Comoé Basin studied by [34], the Dimbokro granitoids have broadly similar geochemical compositions. However, a few particularities warrant attention: the biotite granites exhibit significantly higher Rb contents (up to 417 ppm), suggesting a more advanced degree of

differentiation or more pronounced crustal contamination.

Negative anomalies in Nb and Ta in multi-element spectra, combined with enrichment in LILE, are robust geochemical signatures of magmas associated with subduction zones [32] [33].

The coexistence, within the same area, of metasediments and granitoids is consistent with recent geodynamic models that envisage the evolution of the Eburna orogeny as involving a subduction phase followed by a collision [35] [36].

Compared with other well-studied lithological units within the Comoé Basin and the broader West African Craton, the Dimbokro metasediments display geochemical signatures closely comparable to those reported from the southeastern Comoé Basin by [24] and from equivalent Birimian basins in Ghana [11] [25], confirming the regional coherence of the Birimian peri-arc depositional system. The granitoids of the Dimbokro region similarly compare well with Birimian calc-alkaline plutonic suites documented elsewhere in the Leo-Man Ridge [1] [2], further supporting their common arc-related origin. Furthermore, the identification of gold-bearing quartz veins traversing the mica schists, combined with the geochemical evidence for arc-related metasediments intruded by I-type granitoids, highlights the favourable metallogenic context of the Dimbokro region. These findings suggest that the gold mineralisation is likely structurally controlled along the contact zones between the metasedimentary country rock and the intrusive granitoids, and may thus provide useful criteria for future mineral exploration targeting in this part of the Comoé Basin.

6. Conclusion

Petrographic and geochemical studies of the metasediments and granitoids in the Dimbokro region have made it possible to reconstruct a coherent two-stage lithological and geodynamic evolution. Stage 1 corresponds to the deposition of metasediments (mica schists, metagrauwacks and quartzites) in a Birimian peri-arc basin, fed by the erosion of continental arc-type volcanic edifices, as evidenced by the CIA values (54 - 79), the intermediate to felsic composition of the protoliths, and the Nb-Ta depletion in the multi-element spectra. Stage 2 corresponds to arc magmatism and granitoid emplacement: subsequently, granitoids (biotite granites, granodiorites and tonalites) were intruded into this older metasedimentary country rock; their mineralogy comprising quartz, plagioclases, potassium feldspars and biotites, their membership of the calc-alkaline series, their Type I peraluminous character and their trace element signature indicate a hybrid mantle-crust origin, within a volcanic arc tectonic environment evolving towards a collisional regime. These results confirm that the Dimbokro region constitutes a representative link in the Eburnean crustal accretion of the West African Craton.

Conflicts of Interest

The authors declare no conflicts of interest regarding the publication of this paper.

References

[1] Doumbia, S., Pouclet, A., Kouamelan, A., Peucat, J.J., Vidal, M. and Delor, C. (1998) Petrogenesis of Juvenile-Type Birimian (Paleoproterozoic) Granitoids in Central Côte-D'ivoire, West Africa: Geochemistry and Geochronology. *Precambrian Research*, **87**, 33-63. https://doi.org/10.1016/s0301-9268(97)00201-5

[2] Gasquet, D., Barbey, P., Adou, M. and Paquette, J.L. (2003) Structure, Sr-Nd Isotope Geochemistry and Zircon U-Pb Geochronology of the Granitoids of the Dabakala Area (Côte D'ivoire): Evidence for a 2.3 Ga Crustal Growth Event in the Palaeoproterozoic of West Africa? *Precambrian Research*, **127**, 329-354. https://doi.org/10.1016/s0301-9268(03)00209-2

[3] McLennan, S.M., Taylor, S.R. and Kröner, A. (1983) Geochemical Evolution of Archean Shales from South Africa. I. The Swaziland and Pongola Supergroups. *Precambrian Research*, **22**, 93-124. https://doi.org/10.1016/0301-9268(83)90060-8

[4] Fedo, C.M., Wayne Nesbitt, H. and Young, G.M. (1995) Unraveling the Effects of Potassium Metasomatism in Sedimentary Rocks and Paleosols, with Implications for Paleoweathering Conditions and Provenance. *Geology*, **23**, 921-924. https://doi.org/10.1130/0091-7613(1995)023<0921:uteopm>2.3.co;2

[5] Cullers, R.L. (2000) The Geochemistry of Shales, Siltstones and Sandstones of Pennsylvanian-Permian Age, Colorado, USA: Implications for Provenance and Metamorphic Studies. *Lithos*, **51**, 181-203. https://doi.org/10.1016/s0024-4937(99)00063-8

[6] Lahtinen, R. (2000) Archaean-Proterozoic Transition: Geochemistry, Provenance and Tectonic Setting of Metasedimentary Rocks in Central Fennoscandian Shield, Finland. *Precambrian Research*, **104**, 147-174. https://doi.org/10.1016/s0301-9268(00)00087-5

[7] Condie, K.C., Lee, D. and Farmer, G.L. (2001) Tectonic Setting and Provenance of the Neoproterozoic Uinta Mountain and Big Cottonwood Groups, Northern Utah: Constraints from Geochemistry, Nd Isotopes, and Detrital Modes. *Sedimentary Geology*, **141**, 443-464. https://doi.org/10.1016/s0037-0738(01)00086-0

[8] Hofmann, A., Bolhar, R., Dirks, P. and Jelsma, H. (2003) The Geochemistry of Archaean Shales Derived from a Mafic Volcanic Sequence, Belingwe Greenstone Belt, Zimbabwe: Provenance, Source Area Unroofing and Submarine versus Subaerial Weathering. *Geochimica et Cosmochimica Acta*, **67**, 421-440. https://doi.org/10.1016/s0016-7037(02)01086-4

[9] Roddaz, M., Debat, P. and Nikiema, S. (2007) Geochemistry of Upper Birimian Sediments (Major and Trace Elements and Nd-Sr Isotopes) and Implications for Weathering and Tectonic Setting of the Late Paleoproterozoic Crust. *Precambrian Research*, **159**, 197-211. https://doi.org/10.1016/j.precamres.2007.06.008

[10] Hofmann, A. (2005) The Geochemistry of Sedimentary Rocks from the Fig Tree Group, Barberton Greenstone Belt: Implications for Tectonic, Hydrothermal and Surface Processes during Mid-Archaean Times. *Precambrian Research*, **143**, 23-49. https://doi.org/10.1016/j.precamres.2005.09.005

[11] Asiedu, D.K., Asong, S., Atta-Peters, D., Sakyi, P.A., Su, B., Dampare, S.B., *et al.* (2017) Geochemical and Nd-Isotopic Compositions of Juvenile-Type Paleoproterozoic Birimian Sedimentary Rocks from Southeastern West African Craton (Ghana): Constraints on Provenance and Tectonic Setting. *Precambrian Research*, **300**, 40-52. https://doi.org/10.1016/j.precamres.2017.07.035

[12] Bessoles, B. (1977) Géologie de l'Afrique. Vol 1: Le Craton Ouest Africain. Mémoires du Bureau de recherches géologiques et minières, No. 88, 402 p. https://openlibrary.org/books/OL4320067M/Ge%CC%81ologie_de_l%27Afrique

[13] Milési, J.P., Feybesse, J.L., Ledru, P., Dommanget, A., Ouedraogo, M.F., Tegyey, M., Calvez, J.Y. and Lagny, P. (1989) Les minéralisations aurifères de l'Afrique de l'Ouest et leur évolution litho structurale au Protérozoïque inférieur. *Chronique de la Recherche Minière*, **497**, 3-98.

[14] Vidal, M. and Alric, G. (1994) The Palaeoproterozoic (Birimian) of Haute-Comoé in the West African Craton, Ivory Coast: A Transtensional Back-Arc Basin. *Precambrian Research*, **65**, 207-229. https://doi.org/10.1016/0301-9268(94)90106-6

[15] Alric, G., Gibert, P. and Vidal, M. (1987) The Problem of Birimian Grauwackes in Côte d'Ivoire: A Review and New Data. The Case of the Comoé Unit. *Proceedings of the Academy of Sciences*, **304**, 289-294.

[16] Delor, C., Diaby, I., Tastet, J.P., Yao, B., Siméon, Y., Vidal, M. and Dommanget, A. (1992) Explanatory Note for the Geological Map of Côte d'Ivoire 1/200,000, Abidjan Sheet. Ministry of Mines and Energy, DMG.

[17] Chapell, B.W. and White, A.J.R. (1974) Two Contrasting Types of Granites. *Pacific Geology*, **8**, 173-174.

[18] Herron, M.M. (1988) Geochemical Classification of Terrigenous Sands and Shales from Core or Log Data. *SEPM Journal of Sedimentary Research*, **58**, 820-829. https://doi.org/10.1306/212f8e77-2b24-11d7-8648000102c1865d

[19] Nesbitt, H.W. and Young, G.M. (1982) Early Proterozoic Climates and Plate Motions Inferred from Major Element Chemistry of Lutites. *Nature*, **299**, 715-717. https://doi.org/10.1038/299715a0

[20] Nesbitt, H.W. and Young, G.M. (1984) Prediction of Some Weathering Trends of Plutonic and Volcanic Rocks Based on Thermodynamic and Kinetic Considerations. *Geochimica et Cosmochimica Acta*, **48**, 1523-1534. https://doi.org/10.1016/0016-7037(84)90408-3

[21] McDonough, W.F. and Sun, S.S. (1995) The Composition of the Earth. *Chemical Geology*, **120**, 223-253. https://doi.org/10.1016/0009-2541(94)00140-4

[22] Taylor, S.R. and McLennan, S.M. (1985) The Continental Crust: Its Composition and Evolution. Blackwell, 312 p.

[23] Roser, B.P. and Korsch, R.J. (1986) Determination of Tectonic Setting of Sandstone-Mudstone Suites Using SiO_2 Content and K_2O/Na_2O Ratio. *The Journal of Geology*, **94**, 635-650. https://doi.org/10.1086/629071

[24] Adingra, M.P.K. (2020) Petrostructural and Geochemical Characterization of the Birimian Formations of the South-Eastern Part of the Comoé Basin (North of Alépé-Southeast of Ivory Coast): Implication on the Geodynamic Evolution. PhD Thesis, University Félix Houphouët Boigny, 220. http://publication.lecames.org/index.php/svt/article/download/1450/827

[25] Feybesse, J.L., Billa, M., Diaby, S., Diallo, S., Egal, E., Le Metour, J., Lescuyer, J.L., Sylla, B.I. and Villeneuve, M. (2004) Explanatory Note on the 1:500,000 Geological and Geotectonic Map of Guinea. BRGM, DNRGH, 60.

[26] Bhatia, M.R. and Crook, K.A.W. (1986) Trace Element Characteristics of Graywackes and Tectonic Setting Discrimination of Sedimentary Basins. *Contributions to Mineralogy and Petrology*, **92**, 181-193. https://doi.org/10.1007/bf00375292

[27] McLennan, S.M., Hemming, S., McDaniel, D.K. and Hanson, G.N. (1993) Geochemical Approaches to Sedimentation, Provenance, and Tectonics. In: Johnsson, M.J. and Basu, A., Eds., *Processes Controlling the Composition of Clastic Sediments*, Geological Society of America, Special Papers 285, 21-40. https://doi.org/10.1130/spe284-p21

[28] Pearce, J.A. and Cann, J.R. (1973) Tectonic Setting of Basic Volcanic Rocks Determined Using Trace Element Analyses. *Earth and Planetary Science Letters*, **19**, 290-300. https://doi.org/10.1016/0012-821x(73)90129-5

[29] Middlemost, E.A.K. (1994) Naming Materials in the Magma/igneous Rock System. *Earth-Science Reviews*, **37**, 215-224. https://doi.org/10.1016/0012-8252(94)90029-9

[30] Wright, J.B., Hastings, D.A., Jones, W.B. and Williams, H.R. (1969) Geology and Mineral Resources of West Africa. Allen & Unwin (Editeurs), 187 p.

[31] Shand, S.J. (1922) The Problem of the Alkaline Rocks. *Proceedings of the Geological Society of South Africa*, **25**, 19-33.

[32] Arculus, R.J., Lapierre, H. and Jaillard, É. (1999) Geochemical Window into Subduction and Accretion Processes: Raspas Metamorphic Complex, Ecuador. *Geology*, **27**, 547-550. https://doi.org/10.1130/0091-7613(1999)027<0547:gwisaa>2.3.co;2

[33] Pearce, J.A., Harris, N.B.W. and Tindle, A.G. (1984) Trace Element Discrimination Diagrams for the Tectonic Interpretation of Granitic Rocks. *Journal of Petrology*, **25**, 956-983. https://doi.org/10.1093/petrology/25.4.956

[34] Koffi, Y.A., Kouamelan, A.N., Kouadio, F.J.L.H., Teha, K.R., Kouassi, B.R. and Koffi, G.R.S. (2018) Pétrographie et origine des métasédiments du domaine SASCA (SW de la Côte d'Ivoire). *International Journal of Innovation and Applied Studies*, **23**, 451-464. https://www.proquest.com/openview/9df96268e640e1dc8d6695b4fcc9087f/1?pq-origsite=gscholar&cbl=2031961

[35] Vidal, M., Gumiaux, C., Cagnard, F., Pouclet, A., Ouattara, G. and Pichon, M. (2009) Evolution of a Paleoproterozoic "Weak Type" Orogeny in the West African Craton (Ivory Coast). *Tectonophysics*, **477**, 145-159. https://doi.org/10.1016/j.tecto.2009.02.010

[36] Baratoux, L., Metelka, V., Naba, S., Jessell, M.W., Grégoire, M. and Ganne, J. (2011) Juvenile Paleoproterozoic Crust Evolution during the Eburnean Orogeny (~2.2-2.0 Ga), Western Burkina Faso. *Precambrian Research*, **191**, 18-45. https://doi.org/10.1016/j.precamres.2011.08.010